




Article

Investigations into the Antifungal, Photocatalytic, and Physicochemical Properties of Sol-Gel-Produced Tin Dioxide Nanoparticles

Sirajul Haq ^{1,*}, Nadia Shahzad ², Muhammad Imran Shahzad ³, Khaled Elmnasri ⁴, Manel Ben Ali ⁵, Alaa Baazeem ⁵, Amor Hedfi ⁵ and Rimsha Ehsan ¹

¹ Department of Chemistry, University of Azad Jammu and Kashmir, Muazaffabad 13100, Pakistan

² US-Pakistan Centre for Advance Studies in Energy, National University of Science and Technology (NUST), Islamabad 44000, Pakistan

³ Nanoscience and Nanotechnology Department, National Centre for Physics (NCP), Islamabad 44000, Pakistan

⁴ Higher institute of Biotechnology, University of Manouba, ISBST, BVBGR-LR11ES31, Biotechpole Sidi Thabet, Ariana 2010, Tunisia

⁵ Department of Biology, College of Science, Taif University, P.O. Box 11099, Taif 21944, Saudi Arabia

* Correspondence: cii_raj@yahoo.com

Abstract: Transmission electron microscopy (TEM), atomic force microscopy (AFM), X-ray diffraction (XRD), energy dispersive X-ray (EDX), scanning electron microscopy (SEM), diffuse reflectance spectroscopy (DRS), and Fourier transform infrared (FTIR) spectroscopy were applied to evaluate the tin dioxide nanoparticles (SnO₂ NPs) amalgamated by the sol-gel process. XRD was used to examine the tetragonal-shaped crystallite with an average size of 26.95 (±1) nm, whereas the average particle size estimated from the TEM micrograph is 20.59 (±2) nm. A dose-dependent antifungal activity was performed against two fungal species, and the activity was observed to be increased with an increase in the concentration of SnO₂ NPs. The photocatalytic activity of SnO₂ NPs in aqueous media was tested using Rhodamine 6G (Rh-6G) under solar light illumination. The Rh-6G was degraded at a rate of 0.96 × 10⁻² min for a total of 94.18 percent in 350 min.

Keywords: antifungal activity; tin dioxide; sol-gel; tetragonal; photocatalysis; solar-light



Citation: Haq, S.; Shahzad, N.; Shahzad, M.I.; Elmnasri, K.; Ali, M.B.; Baazeem, A.; Hedfi, A.; Ehsan, R. Investigations into the Antifungal, Photocatalytic, and Physicochemical Properties of Sol-Gel-Produced Tin Dioxide Nanoparticles. *Molecules* **2022**, *27*, 6750. <https://doi.org/10.3390/molecules27196750>

Academic Editors: Nagaraj Basavegowda and Kwang-Hyun Baik

Received: 17 September 2022

Accepted: 30 September 2022

Published: 10 October 2022

Publisher's Note: MDPI stays neutral with regard to jurisdictional claims in published maps and institutional affiliations.



Copyright: © 2022 by the authors. Licensee MDPI, Basel, Switzerland. This article is an open access article distributed under the terms and conditions of the Creative Commons Attribution (CC BY) license (<https://creativecommons.org/licenses/by/4.0/>).

1. Introduction

The fungi are the heterotrophic eukaryotes that are unable to make their own food. These multicellular eukaryotes are ubiquitous, thus fungal infections are common throughout the world. In humans, fungal infections are mostly caused when a fungus attacks over the low immunity area of the body that is adaptive to it. Fungi can live in plants, soil, air, water and in human body naturally [1]. Like other microbial organisms, some fungi are harmful, while some are useful. When a harmful fungus attacks the human body the victim complains of itching, swelling and redness depending on the attacked area of the body. Fungi cause both surface and systemic infections and can have lethal outcomes if diagnosed at the later stages [2].

The attack of pathogens, especially fungi, has put the food security at risk and, according to a rough estimate, almost one-third of annual crops are lost due to the attack and invasion of these harmful pathogens [3]. Economically valuable crops are harmed by pathogenic fungi at pre-harvest or post-harvest stages. The fungicides used for their control are imparting a damaging effect on both humans and the environment. Thus, silver nanoparticles have been reported for the control of phytopathogenic fungi as these NPs cause growth restriction of such fungi without disturbing the environment [4]. Solvothermally synthesized gold NPs have also been advertised for antifungal activity against the candida species [5]. The ZnO NPs synthesized by biological methods using extracts like *Allium cepa*, garlic, parsley, *Dolichos lablab* L. and *Sphingomonas paucimobilis* have also been

reported in the literature showing affective fungal growth inhibition, mostly of candida species [6].

The reduction of organic dyes from water reservoirs are a major concern in this industrial world and the damages related to the presence of organic substances in aquatic environments is unmeasurable. Rhodamine 6G is a heterocyclic cationic polar dye belonging to the Xanthene family and has strong absorption in the visible region [7]. Rhodamine 6G is used in the field of hydraulics as fluorescent tracer to visualize flow patterns and also is commonly used also as a sensitizer. The discharge of rhodamine 6G into the aqueous medium is harmful for humans and longer term exposure results in multiple health issues such as vomiting, increase in heart rate, lung cancer, skin cancer and, in some cases, delay in physiological development. Therefore, it is highly necessary to degrade organic substances from waste water before they accumulate in the environment causing irreversible damage [8]. Photocatalysis involves the production of the hydroxyl radical and superoxide anion, which are generated by absorption of radiation by the catalyst. SnO₂ is widely used due to its nontoxic effect, stability and strong oxidizing properties [9].

SnO₂ is one of the best semiconductors, having shape dependent properties and a band gap of 3.6 eV [10]. The SnO₂ NPs have potential to degrade organic dye and help in the protection of the environment [11]. At the nano-scale, SnO₂ exhibits exceptional properties owing to its high surface area to volume ratio, which makes it a unique photocatalyst [12]. The nano-sized SnO₂ is an efficient catalyst for oxidation of organic compounds due to the presence of a high number of surface active groups [13]. The large surface area of SnO₂ NPs having a size below 10 nm has more reaction sites, which increases the photocatalytic efficacy, which might also be attributed to the large electron-hole pair separation [14]. The Sol-gel synthesis of SnO₂ NPs is preferred over other methods, because it is easy to handle, provides better control over the particle size and is economic [15].

The current research concerns the sol-gel synthesis of SnO₂ NPs for antifungal activity and photodegradation of rhodamine 6G. The as-manufactured SnO₂ NPs were characterized by manipulating SEM, XRD, EDX, AFM, TEM, DRS and FTIR spectroscopy. The antifungal activity was performed against the selected fungus species using the Agar well diffusion method. The selection of fungi is purely based on the availability of the fungal strain and its toxicity. The degradation of rhodamine 6G was brought under solar light irradiation and the reaction parameters were determined by a set of mathematical equations.

2. Results

2.1. XRD Analysis

The XRD pattern of SnO₂ NPs exhibited in Figure 1 shows the characteristic peaks along with corresponding hkl values for SnO₂ at 2θ 26.34 (110), 33.68 (101), 38.06 (200), 52.00 (211) and 65.21 (301), which harmonized with the diffraction bands listed in the JCPDS card no. 01-077-0449 assigned to the cubic geometry of crystals. The noisy XRD pattern with broad diffraction band suggests the presence of both amorphous and crystalline phase in the sample [16]. The sharpness of diffraction bands suggest that some portion of the synthesized material is highly crystalline while the varied width and intensity shows a wide range distribution of crystallite size. The average crystallite size for SnO₂ NPs enumerated by Debye-Scherrer equation is 26.95 nm with 0.39% imperfection, found in the crystal.

2.2. EDX Analysis

In the EDX spectrum of SnO₂ NPs (Figure 2), O is responsible for the peak at 0.3 keV, while Sn is responsible for a series of sharp bands in the 3.5–4 keV range, as well as a very tiny signal at 2.6 due to the presence of Cl. According to the EDX analysis, the synthesized SnO₂ NPs have a stoichiometric composition of Sn and O, with a trace of Cl as an impurity. According to EDX statistics, Sn, O, and Cl have weight percentages of 78.7, 20.2 and 1.1 percent, respectively.

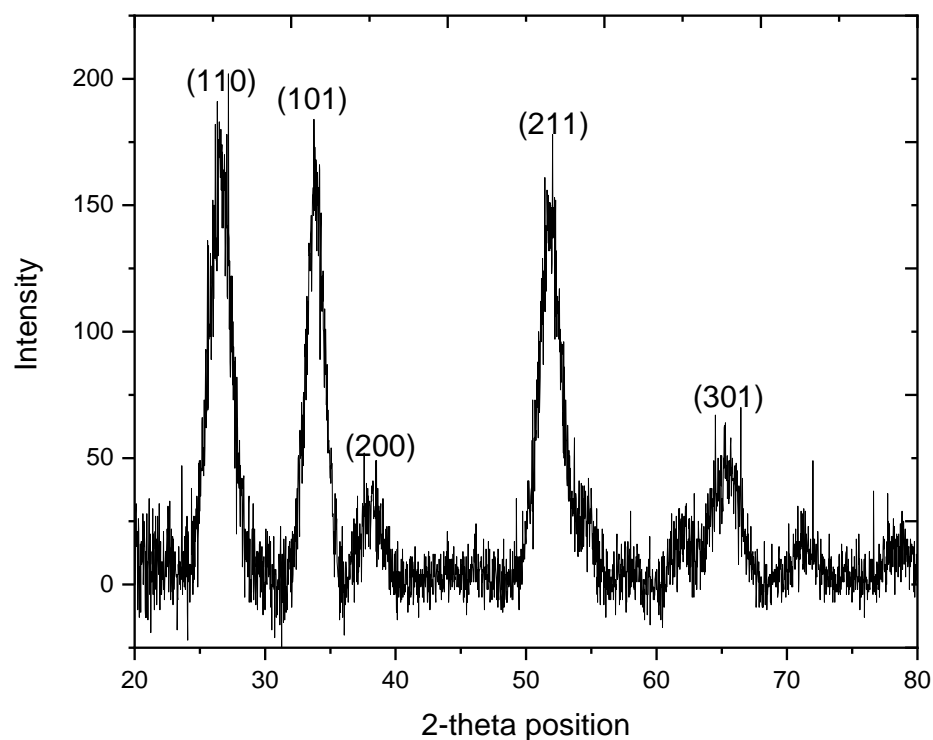


Figure 1. XRD pattern of SnO₂ NPs.

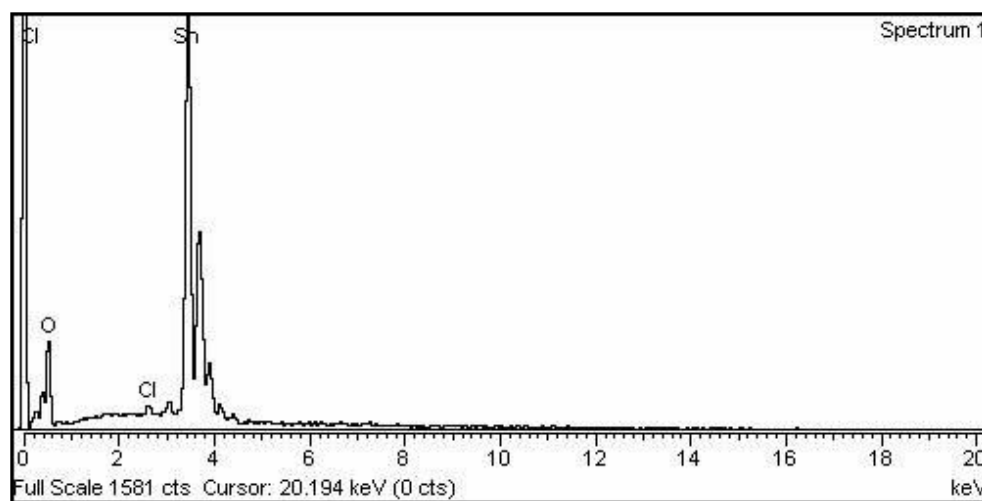


Figure 2. EDX pattern of SnO₂ NPs.

2.3. SEM Analysis

The structural analysis of SnO₂ NPs was carried out via SEM as shown in the low and high magnified micrographs (Figure 3a,b). The images reveal that flat shaped particles of different size are formed by the aggregation of small particles. Each flat shaped particle constitutes 2 to 9 small particles depending upon the size, and the cracks observed in the flat shaped particles are actually the boundaries of the aggregated particles. The size of the flat shaped particles predicted from SEM micrographs range from 78 to 114 nm with an average size of 98.56 nm.

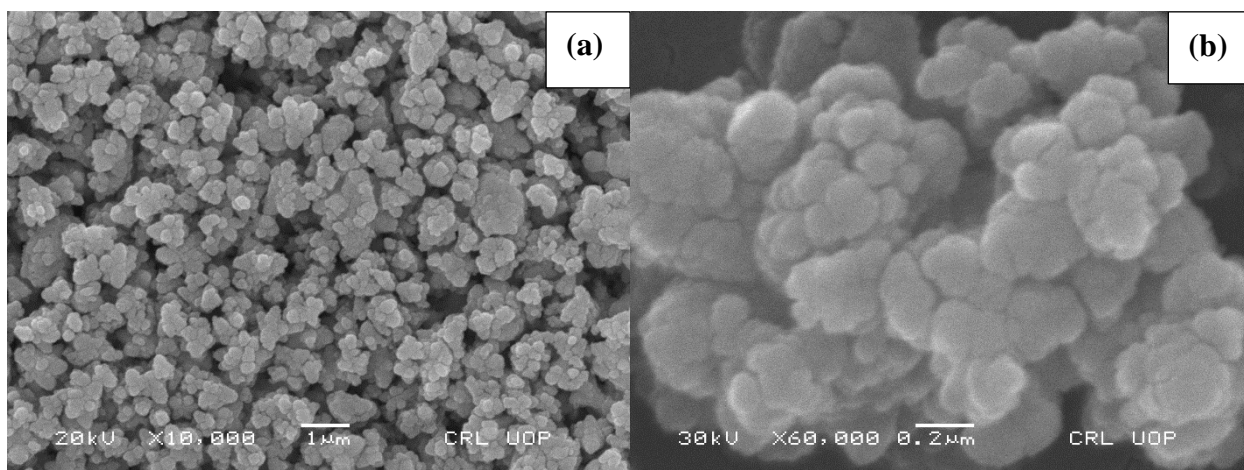


Figure 3. SEM micrographs of SnO₂ NPs. (a) $\times 10,000$; (b) $\times 60,000$.

2.4. TEM Analysis

The TEM micrograph SnO₂ NPs shown in Figure 4, exhibits two portions; one portion is formed due to the accumulation of the particles over one another forming a dark structure, whereas in the other portion the particles are somewhat evenly distributed and are closely connected with each other, leading to the formation of network structure. Although the shape of the particles are not uniform, many of the particles possess nearly spherical shape. It is also seen that the surface of the particles are smooth and have a wide range of size distribution. The particles' size measured by ImageJ software ranges from 13.24 nm to 30.88 nm with an average size of 20.59 nm.

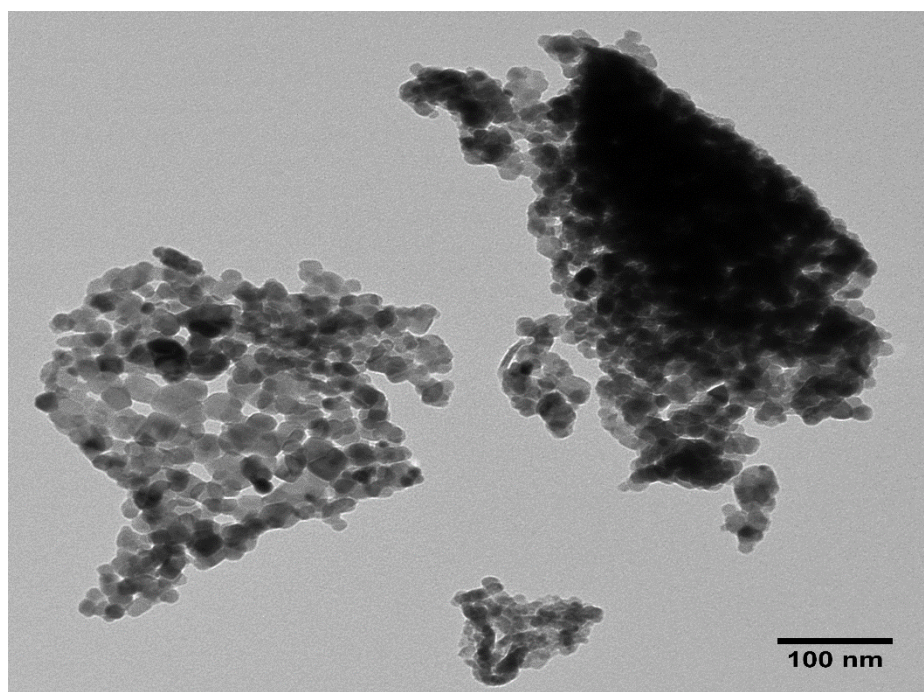


Figure 4. TEM micrograph of SnO₂ NPs.

2.5. AFM Analysis

The distribution of SnO₂ NPs of various sizes and shapes was analyzed via AFM in both 2-dimensions and 3-dimensions as shown in Figure 5. It is seen that the small particles are fused together, leading to the formation of bunch like structures. However, many tiny individual particles are also seen in the micrographs. The density of the particle

is $0.920/\mu\text{m}^2$ whereas the height of the particles ranges from 7.93 to 41.44 nm with average height of 23.95 nm. The particles' diameters, i.e., between 55.09 and 101.60 nm, with an average diameter of 72.73 nm.

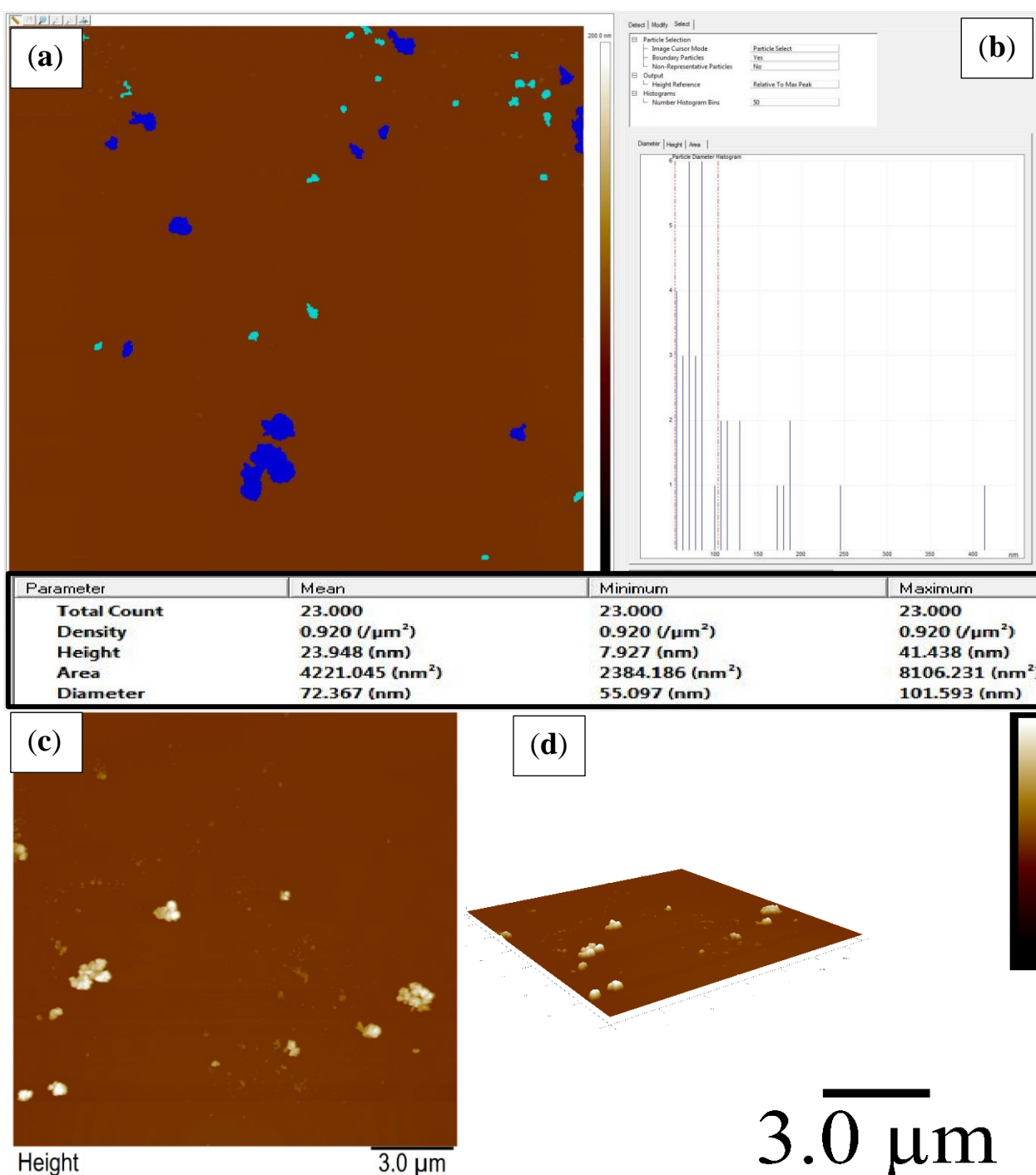


Figure 5. Selected area (a), histogram (b), 2-D (c), and 3-D (d) AFM micrographs of SnO_2 NPs.

2.6. DRS Analysis

The DRS spectrum of SnO_2 NPs (inset: Figure 6) shows greater absorbance in the UV range and a clear decrease was seen in absorbance with increasing wavelength, except for a depth occurring in the boundary line UV and visible region, which might be due to some structural defects. The Tauc plot (Figure 4) was drawn to calculate the band gap energy and was noted to be 3.65 eV, almost similar to that reported in the literature [17].

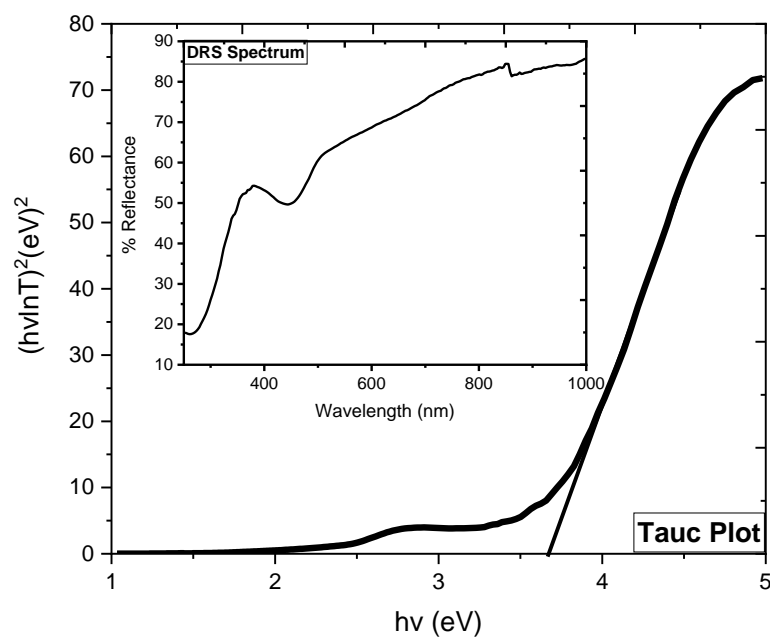


Figure 6. Tauc plot (inset: DRS spectrum) of SnO₂ NPs.

2.7. FTIR Analysis

The stretching and bending vibrations of the hydroxyl group are responsible for a broad band centered at 3248 cm⁻¹ and another peak at 1627.90 cm⁻¹ in the FTIR spectrum of SnO₂ NPs (Figure 7) [18]. The signal at 1383.31 cm⁻¹ confirmed the existence of NO₃ in the sample, which might be attributable to the use of Sn(NO₃)₂ as a precursor in the synthesis. The peaks at 1140.44 and 1015.11 cm⁻¹ are caused by Sn-OH crystal lattice vibrations [19]. The wide band in the range from 761–513 cm⁻¹ is formed by the fusion of two bands at 692 and 601 cm⁻¹, which are ascribed to Sn-O-Sn and Sn-O vibrations, respectively [10].

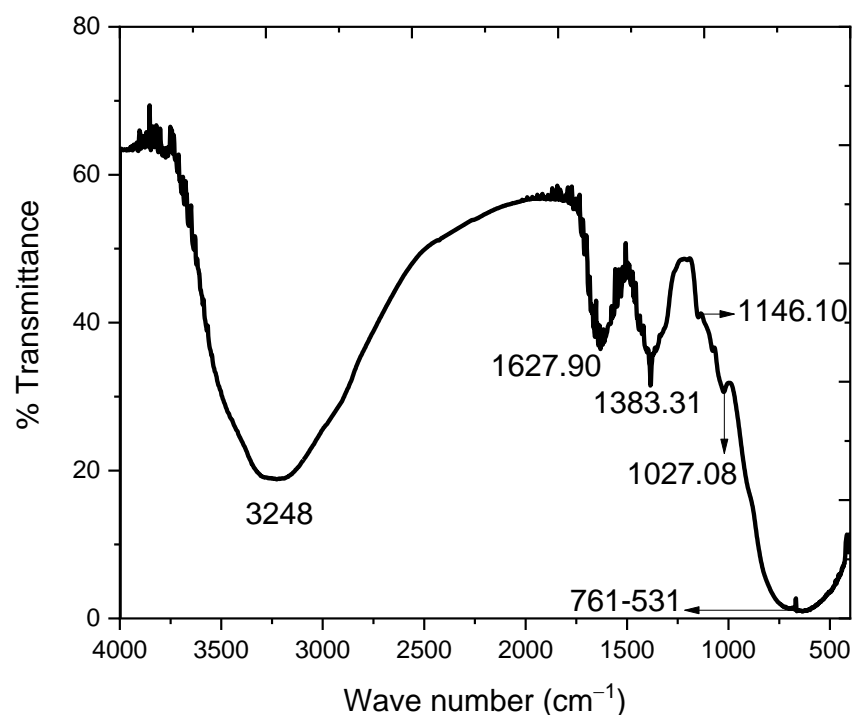


Figure 7. FTIR spectrum of SnO₂ NPs.

2.8. Antifungal Study

The antifungal activity of SnO₂ NPs was scrutinized against the selected fungi at different concentrations as shown in Figure 8 and the obtained data is tabulated in Table 1. The results shows that the activity of SnO₂ NPs increased along with increase in concentration in the well. At 40 µg/mL, no activity was shown against both fungi, but onward increase in concentration significantly inhibits fungus growth and the highest activity was found at 100 µg/mL. However, the activity of SnO₂ NPs was found to be less than the activity of the positive control, 6.1 mm and 6.3 mm for both species, respectively. The solvent was utilized as negative control and has no effect on the activity of SnO₂ NPs and positive control. The increase in the activity with increasing concentration is attributed to the larger number of particles present in the suspension, that provide more binding sites to interact with the fungi. It has been reported that most of the antifungal agents act in a non-specific way, either changing the permeability of the cell wall and cell membrane or disturbing the cytoplasmic composition/leakage of cytoplasmic fluid. They also act as enzyme inhibitors altering the biochemical nature, which leads to the death of organisms [20].

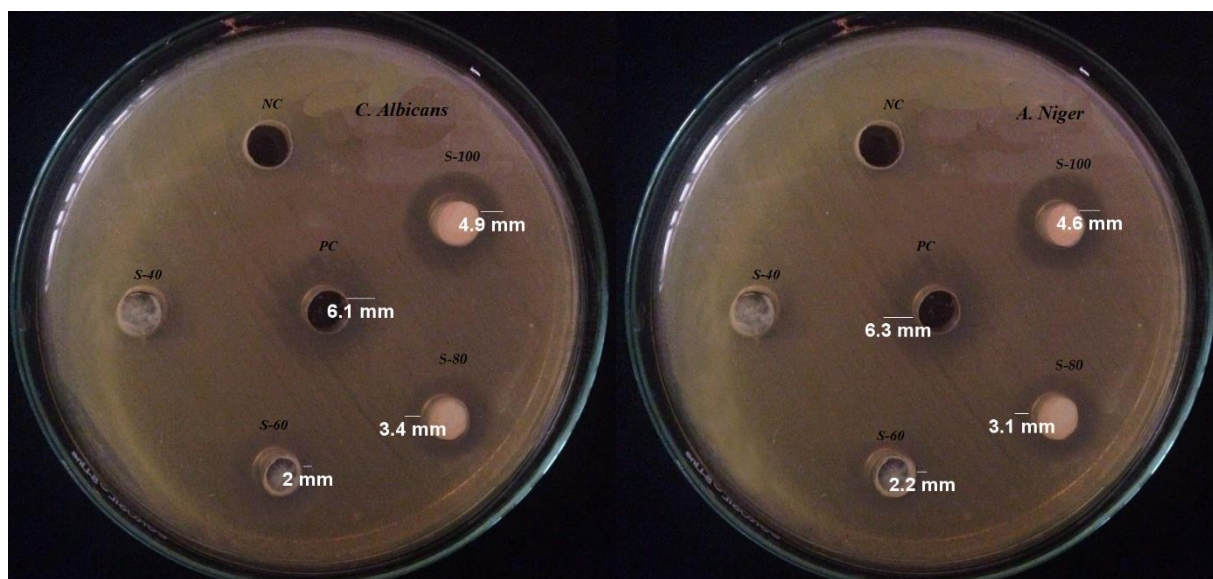


Figure 8. Experimental photographs of antifungal activity of SnO₂ NPs against selected fungi at different concentrations.

Table 1. Antifungal activity of SnO₂ NPs against the selected fungi and statistical analysis.

Species	Concentration (µg/mL)	Inhibition Zone (mm)	PS	NC	Variance (S ²)	Standard Deviation (S)	Pearson Constant (<0.05)
<i>C. Albicans</i>	40	0	6.1	0	1.72	1.3	0.0054
	60	2					
	80	3.4					
	100	4.9					
<i>A. Niger</i>	40	0	6.3	0	1.5	1.2	0.0055
	60	2.2					
	80	3.1					
	100	4.6					

2.9. Photocatalytic Study

In the presence of SnO₂ NPs, the solar light induced degradation of Rh-6G was carried out in aqueous medium, and the visual deterioration was monitored by the fading hue of the dye solution over time. The degradation process was investigated experimentally

using a double beam spectrophotometer, where a decrease in the absorbance maxima at 526 nm was noted as time passed, and the results are presented in Figure 9a [21]. The percentage degradation of Rh-6G was calculated using Equation (1), and the result was 94.18 percent in 330 min (Figure 9b, which was greater than previously reported [22]). The Langmuir-Hinshelwood kinetic model (Equation (2)) was manipulated to investigate the photocatalytic reaction kinetics, where the initial and end concentrations of Rh-6G are C_0 and C_e , respectively, and k and t are the apparent constants [23]. The straight line produced by plotting $\ln C_0/C_e$ versus time (Figure 9c) with r^2 values of 0.844 suggests that the photocatalytic process is pseudo-first order. The photo-degradation rate constants for Rh-6G via SnO₂ NPs are enumerated from the slope of linear plots and are $0.999 \times 10^{-2} \text{ min}^{-1}$.

$$\% \text{ Degradation} = \frac{C_0 - C_t}{C_0} \times 100 \quad (1)$$

$$\ln(C/C_0) = -kt \quad (2)$$

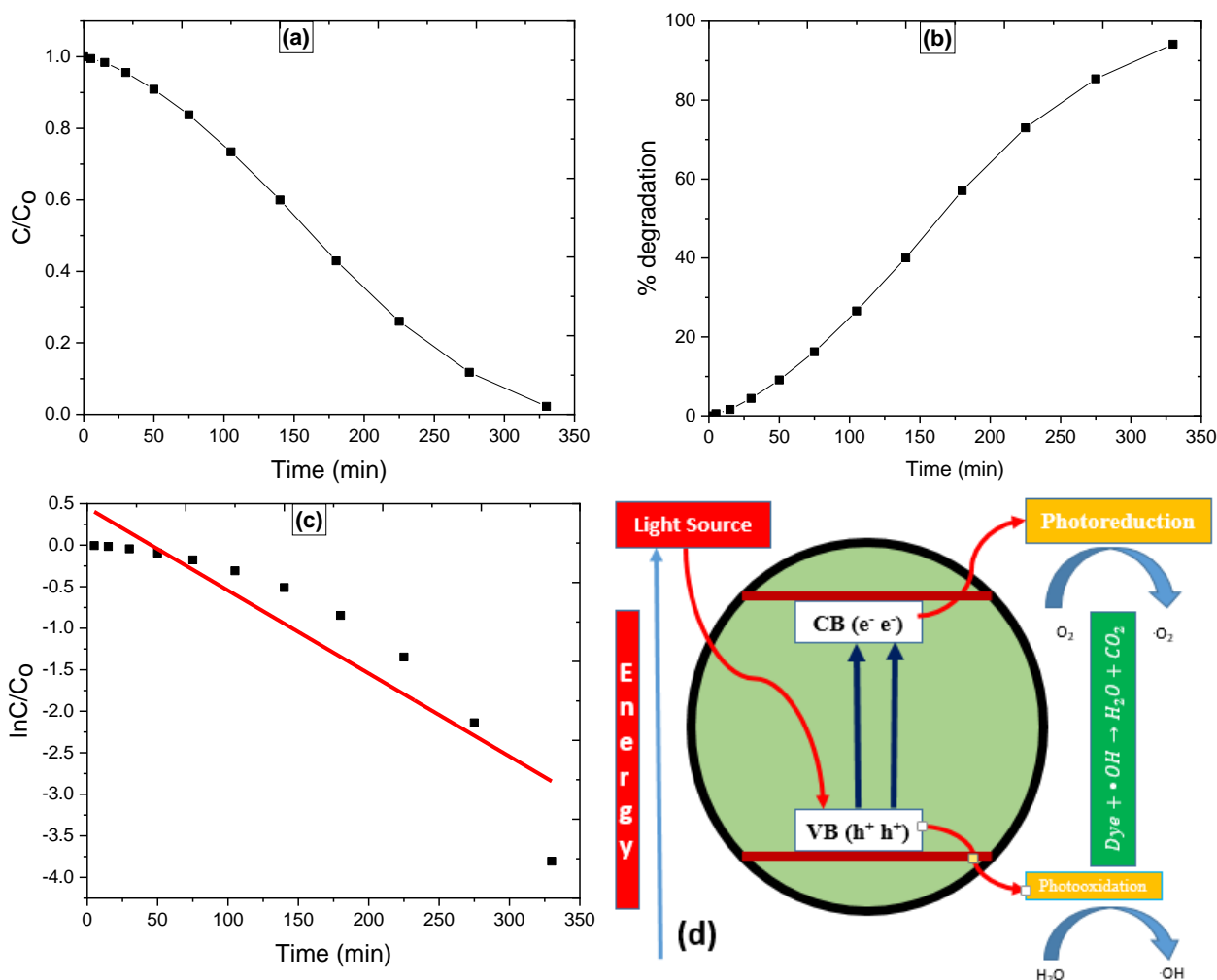


Figure 9. Photocatalytic parameters including, (a) = degradation profile, (b) = percentage degradation, (c) = kinetic plot and (d) = electron excitation and hole creation mechanism.

When light with an energy equal to or greater than the SnO₂ NPs band gap reaches the surface, the outermost electron is excited to the conduction band (CB), leaving a positive hole in the valence band (VB), as illustrated in Figure 9d. The positive holes interact with the water/hydroxyl group to produce hydroxyl radicals, which are powerful oxidizers that convert Rh-6G to H₂O and CO₂ [23]. The super oxide radicals, on the other hand, are

produced by the interaction of an excited electron with absorbed oxygen, providing an additional source of hydroxyl radical and speeding up the oxidation of Rh-6G [24].

3. Materials and Methods

3.1. Materials

Sigma-Aldrich provided analytical grade chemicals such as $\text{Sn}(\text{NO}_3)_2$, hydrochloric acid and $\text{C}_2\text{H}_5\text{OH}$, which were utilized without any further purification. Deionized water was utilized to make all of the working solutions, and 15% nitric acid solution was manipulated to clean all the glassware before being bathed with the deionized water.

3.2. Synthesis of SnO_2 NPs

A 10 mM solution of $\text{Sn}(\text{NO}_3)_2$ was produced on dissolving 1.21 g in 500 mL deionized water, and 80 mL from this solution was combined with 20 mL of ethanol for the fabrication of SnO_2 NPs. The reaction mixture was stirred (250 rpm) and heated at 50 °C for 40 min at pH 2.5 by adding HCl solution. After forming a white gel and ageing it for 24 h, it was washed using deionized water and dried at 150 °C. For later usage, the white powder was kept in an airtight plastic bottle.

3.3. Characterization

The Panalytical X-Pert Pro X-ray diffraction model was used to investigate the crystal property, with XRD analysis in the 20°–80° 2-theta range and the Debye-Scherrer equation used to compute crystallite size. For morphological examination, a scanning electron microscope model JEOL 5910 (Japan) was utilized, and the particle size was determined using ImageJ software. At 20 keV, the energy dispersive X-ray model INCA 200 (UK) was utilized to assess the percentage composition and purity. The band gap energies were calculated for a reflectance spectrum collected using the diffuse reflectance spectroscopy model lambda 950 with a desegregating sphere in the wavelength range of 200–2500 nm. For the identification of surface functional groups, FTIR spectra in the region of 4000–400 cm^{-1} were acquired using a Nicolet 6700 (USA) spectrometer.

3.4. Antifungal Assay

The antifungal screening of SnO_2 NPs against *Aspergillus niger* (ATCC#16404) and *Candida albicans* (ATCC#10231) was carried out using the Agar well diffusion method. Four SnO_2 NPs suspensions were prepared by ultrasonic dispersion of 40, 60, 80 and 100 μg in 1 mL. The well was bored in the media using a sterile borer and each well individually was equipped with 100 μL of each suspension and was incubated at room temperature. The zone of inhibition was computed in millimeters (mm) after 7 days as the activity of SnO_2 NPs against the fungal species. The statistical analysis was carried out with 95% confidence interval using Microsoft Excel 2013 (Las Vegas, NV, USA).

3.5. Photocatalytic Assay

The experiment was carried out in a double-walled Pyrex reactor with a water input and exit under solar light. To avoid sun contact, 50 mL of Rh-6G solution (15 ppm) and 20 mg of catalyst (0.4 g/L) were added to the reactor for each reaction, and the reactor was enclosed in aluminum foil. After exposing the reaction to sunlight for a while, 3 mL of the sample was subjected to centrifugation for 4 min at 4000 rpm and examined with a double beam spectrophotometer (Thermo Spectronic UV 500). There was a decrease in absorbance maxima as the time passed.

4. Conclusions

A facile and single-step sol-gel process was operated for the fabrication of SnO_2 NPs, which was found to be more economical and time saving, with no use of toxic and expensive templates. Different methods were used to investigate the physicochemical characteristics, which revealed the development of a well-crystalline cubic-shaped crys-

tallite in the nano-metric range. The different shapes and morphology of SnO₂ NPs were seen in microstructural analysis. The larger grain size might be due to the aggregation of various small particles. The EDX analysis confirmed the desired composition SnO₂ NPs and the presence of Cl as impurity in the sample might be due to the improper washing process. A significant antifungal activity was shown by the SnO₂ NPs against both the fungal species at higher concentrations. The 94.18 percent Rh-6G degraded in 330 min at a rate of 0.999×10^{-2} per min. The SnO₂ NPs' improved photocatalytic activity against Rh-6G was due to their tiny size and porous structure, as revealed by XRD, AFM and TEM analyses.

Author Contributions: Conceptualization, S.H. and M.I.S.; methodology, S.H., R.E. and N.S.; software, A.H. and M.I.S.; validation, M.B.A., M.I.S. and K.E.; formal analysis, S.H. and R.E.; investigation, N.S.; resources, M.I.S. and S.H.; data curation, K.E.; writing—original draft preparation, R.E. and S.H.; writing—review and editing, A.B., A.H., K.E. and M.B.A.; visualization, M.I.S.; supervision, S.H. and A.B.; project administration, N.S.; funding acquisition, A.B., M.B.A., A.H. and K.E. All authors have read and agreed to the published version of the manuscript.

Funding: This research was funded by Taif University Researchers Supporting Project number (TURSP-2020/295), Taif University, Taif, Saudi Arabia.

Institutional Review Board Statement: Not applicable.

Informed Consent Statement: Not applicable.

Data Availability Statement: All the data is enclosed in the manuscript.

Conflicts of Interest: The authors declare no conflict of interest.

Sample Availability: Samples of the compounds are available from the authors.

References

1. Alananbeh, K.M.; Al-Refaei, W.J.; Al-Qodah, Z. Antifungal Effect of Silver Nanoparticles on Selected Fungi Isolated from Raw and Waste Water. *Indian J. Pharm. Sci.* **2017**, *79*, 559–567. [[CrossRef](#)]
2. Mahdi, B.M. Review of Fungal Infection in Human Beings and Role of COVID-19 Pandemic. *Indian J. Forensic Med. Toxicol.* **2021**, *15*, 887–897.
3. Hashem, A.H.; Abdelaziz, A.M.; Askar, A.A.; Fouda, H.M.; Khalil, A.M.A.; Abd-Elsalam, K.A.; Khaleil, M.M. Bacillus megaterium-mediated synthesis of selenium nanoparticles and their antifungal activity against rhizoctonia solani in faba bean plants. *J. Fungi* **2021**, *7*, 195. [[CrossRef](#)]
4. Al-Otibi, F.; Perveen, K.; Al-Saif, N.A.; Alharbi, R.I.; Bokhari, N.A.; Albasher, G.; Al-Otaibi, R.M.; Al-Mosa, M.A. Biosynthesis of silver nanoparticles using Malva parviflora and their antifungal activity. *Saudi J. Biol. Sci.* **2021**, *28*, 2229–2235. [[CrossRef](#)] [[PubMed](#)]
5. Ahmad, T.; Wani, I.A.; Lone, I.H.; Ganguly, A.; Manzoor, N.; Ahmad, A.; Ahmed, J.; Al-Shihri, A.S. Antifungal activity of gold nanoparticles prepared by solvothermal method. *Mater. Res. Bull.* **2013**, *48*, 12–20. [[CrossRef](#)]
6. Abomuti, M.A.; Danish, E.Y.; Firoz, A.; Hasan, N.; Malik, M.A. Green synthesis of zinc oxide nanoparticles using salvia officinalis leaf extract and their photocatalytic and antifungal activities. *Biology* **2021**, *10*, 1075. [[CrossRef](#)]
7. Pino, E. Photocatalytic Degradation of Aqueous Rhodamine 6G Using Supported TiO₂ Catalysts. A Model for the Removal of Organic Contaminants from Aqueous samples. *Front. Chem.* **2020**, *8*, 365. [[CrossRef](#)]
8. Suwunwong, T.; Patho, P.; Choto, P.; Phoungthong, K. Enhancement the rhodamine 6G adsorption property on Fe₃O₄-composited biochar derived from rice husk. *Mater. Res. Express* **2020**, *7*, 025511. [[CrossRef](#)]
9. Silva, L.C.; Barrocas, B.; Jorge, M.E.M. Photocatalytic Degradation of Rhodamine 6G using TiO₂/WO₃ Bilayered Films Produced by Reactive Sputtering. In Proceedings of the 6th International Conference on Photonics, Optics and Laser Technology, Funchal, Portugal, 25–27 January 2018; pp. 334–340. [[CrossRef](#)]
10. Haq, S.; Rehman, W.; Waseem, M.; Shah, A.; Khan, A.R. Green synthesis and characterization of tin dioxide nanoparticles for photocatalytic and antimicrobial studies. *Mater. Res. Express* **2020**, *7*, 025012. [[CrossRef](#)]
11. Surendhiran, K.C.S.S.; Kumar, P.M.; Kumar, E.R.; Khadar, Y.A.S. Green synthesis of SnO₂ nanoparticles using Delonix elata leaf extract: Evaluation of its structural, optical, morphological and photocatalytic properties. *SN Appl. Sci.* **2020**, *2*, 1735. [[CrossRef](#)]
12. Garrafa-galvez, H.E.; Nava, O.; Soto-robles, C.A.; Vilchis-nestor, A.R. Green synthesis of SnO₂ nanoparticle using Lycopersicon esculentum peel extract. *J. Mol. Struct.* **2019**, *1197*, 354–360. [[CrossRef](#)]
13. Adnan, R.; Razana, N.A.; Rahman, I.A.; Farrukh, M.A. Synthesis and Characterization of High Surface Area Tin Oxide Nanoparticles via the Sol-Gel Method as a Catalyst for the Hydrogenation of Styrene Synthesis and Characterization of High Surface Area Tin Oxide Nanoparticles via the Sol-Gel Method as a Catal. *J. Chin. Chem. Soc.* **2010**, *57*, 222–229. [[CrossRef](#)]

14. Viet, P.V.; Thi, C.M.; Hieu, L.V. The High Photocatalytic Activity of SnO₂ Nanoparticles Synthesized by Hydrothermal Method. *J. Nanomater.* **2016**, *2016*, 4231046. [[CrossRef](#)]
15. Suvaitha, P.; Selvam, S.; Ganesan, D.; Rajangam, V.; Raji, A. Green Synthesis of SnO₂ Nanoparticles for Catalytic Degradation of Rhodamine B. *Iran. J. Sci. Technol. Trans. A Sci.* **2020**, *44*, 661–676. [[CrossRef](#)]
16. Haq, S.; Rehman, W.; Rehman, M. Modeling, Thermodynamic Study and Sorption Mechanism of Cadmium Ions onto Isopropyl Alcohol Mediated Tin Dioxide Nanoparticles. *J. Inorg. Organomet. Polym. Mater.* **2020**, *30*, 1197–1205. [[CrossRef](#)]
17. Gajendiran, J.; Rajendran, V. Synthesis and Characterization of Ultrafine SnO₂ Nanoparticles via Solvothermal Process. *Int. J. Phys. Appl.* **2010**, *2*, 45–50.
18. Yao, W.; Wu, S.; Zhan, L.; Wang, Y. Two-dimensional porous carbon-coated sandwich-like mesoporous SnO₂/graphene/mesoporous SnO₂ nanosheets towards high-rate and long cycle life lithium-ion batteries. *Chem. Eng. J.* **2019**, *361*, 329–341. [[CrossRef](#)]
19. Haq, S.; Rehman, W.; Waseem, M.; Rehman, M.U.; Khan, B. Adsorption of Cd²⁺ ions onto SnO₂ nanoparticles synthesized via sol-gel method: Physicochemical study. *Mater. Res. Express* **2019**, *6*, 105035. [[CrossRef](#)]
20. Anjaneyulu, Y.; Rao, R.P. Preparation, characterization and antimicrobial activity studies on some ternary complexes of Cu(II) with acetylacetone and various salicylic acids. *Synth. React. Inorg. Met.-Org. Chem.* **1986**, *16*, 257–272. [[CrossRef](#)]
21. Manjula, N.; Selvan, G.; Balu, A.R. Photocatalytic Performance of SnO₂:Mo Nanopowders Against the Degradation of Methyl Orange and Rhodamine B Dyes Under Visible Light Irradiation. *J. Electron. Mater.* **2019**, *48*, 401–408. [[CrossRef](#)]
22. Shah, A.; Haq, S.; Rehman, W.; Muhammad, W.; Shoukat, S.; Rehman, M. Photocatalytic and antibacterial activities of Paeonia emodi mediated silver oxide nanoparticles. *Mater. Res. Express* **2019**, *6*, 045045. [[CrossRef](#)]
23. Haq, S.; Shoukat, S.; Rehman, W.; Waseem, M.; Shah, A. Green fabrication and physicochemical investigations of zinc-cobalt oxide nanocomposite for wastewater treatment. *J. Mol. Liq.* **2020**, *318*, 114260. [[CrossRef](#)]
24. Ahmad, M.; Rehman, W.; Khan, M.M.; Qureshi, M.T.; Gul, A.; Haq, S.; Ullah, R.; Rab, A.; Mena, F. Phytogenic fabrication of ZnO and gold decorated ZnO nanoparticles for photocatalytic degradation of Rhodamine B. *J. Environ. Chem. Eng.* **2021**, *9*, 104725. [[CrossRef](#)]